The 56th International October Conference on Mining and Metallurgy
22–25 October 2025, Bor Lake, Bor, Serbia
www.ioc.tfbor.bg.ac.rs

DOI: 10.5937/IOC25273L
Original scientific paper

NUMERICAL SIMULATION OF TEMPERATURE FIELD IN A ROTARY HEARTH FURNACE UNDER INFRARED−ASSISTED HEATING CONDITIONS

Xiaohua Liu[1a], Renhao Tian[1b], Yang You[1c], Zhixiong You[1d]*, Xuewei Lv[1e]

College of Materials Science and Engineering, Chongqing University, Chongqing 400044, China.
[1a] liuxiaohua@stu.cqu.edu.cn, 0009-0001-7491-7722
[1b] trh17843610794@163.com, 0009-0000-5443-0733
[1c] youyang@cqu.edu.cn, 0000-0002-5403-0673
[1d] youzx@cqu.edu.cn, 0000-0002-4405-7004
[1e] lvxuewei@cqu.edu.cn, 0000-0003-1690-4373

Abstract

In steel production, significant quantities of steel dust and sludge are generated, among which iron- and zinc-bearing residues hold high recycling potential. Currently, the rotary hearth furnace (RHF) process is one of the most widely used technologies for treating such byproducts in the steel industry. This study employs Fluent-based numerical simulations to analyze the temperature distribution in an RHF under infrared-assisted heating, assessing the feasibility of infrared integration and its potential to reduce carbon emissions. The results indicate that infrared-assisted heating significantly enhances the RHF system's thermal efficiency.

Keywords : *RHF, infrared−assisted heating, Numerical simulations, Reducing carbon emissions*

1. INTRODUCTION

Steel Steelmaking dust sludge, a solid waste byproduct derived from dry and wet flue gas purification processes in iron and steel manufacturing, constitutes 8%–12% of China's annual steel production by mass [1]. Notably, 20%–30% of this residue is classified as iron-zinc-bearing dust sludge due to its elevated concentrations of iron, zinc, potassium, sodium, and other metallic elements [2,3]. Current disposal practices such as open-air stockpiling or landfilling not only impose environmental hazards and land-use inefficiencies but also squander the resource recovery potential of these metal-rich wastes [4,5,6]. The rotary hearth furnace (RHF) process, recognized for its operational efficiency and feedstock versatility, has emerged as the predominant treatment method for iron-zinc-bearing sludge [7,8]. However, conventional RHF systems suffer from excessive carbon emissions and suboptimal chamber space utilization, limitations stemming from their reliance on gas-fired combustion—a heating method with inherent inefficiencies and a substantial carbon footprint.

To mitigate these challenges, improving thermal efficiency while minimizing gas consumption is critical. Infrared-assisted heating, an external energy field technology, presents a promising solution owing to its high thermal efficiency, material penetration capacity, and carbon-neutral operation, all of which are well-documented in industrial applications [9,10]. This study utilizes computational fluid dynamics (CFD) via ANSYS Fluent to simulate temperature field distributions within RHF systems under both gas combustion and infrared-assisted heating conditions. The objective is to assess the feasibility of infrared integration for enhancing RHF thermal performance and reducing carbon emissions.

2. EXPERIMENTAL

2.1 Geometry model of RHF

This study developed a full–scale computational model of RHF from an integrated steel enterprise, as depicted in Figure 1. Specifically, Figure 1(a) illustrates the geometric configuration of the RHF model, while Figure1(b) details its internal structural characteristics. The Rotary Hearth Furnace (RHF) model has a diameter of 30 m and incorporates an annular furnace chamber with a width of 5 m and a height of 1.5 m. Infrared radiation tubes, each with a diameter of 50 mm, are symmetrically installed on both lateral inner walls of the chamber. The central axes of these tubes are positioned 500 mm above the furnace hearth. To reflect operational configurations, the furnace is divided circumferentially into six functional zones: one preheating section and five reduction sections (I–V). Each zone contains a distinct number of burners aligned along the mid-height plane of the lateral walls. These burners are designed to inject gas-air mixtures, enabling controlled combustion heating.

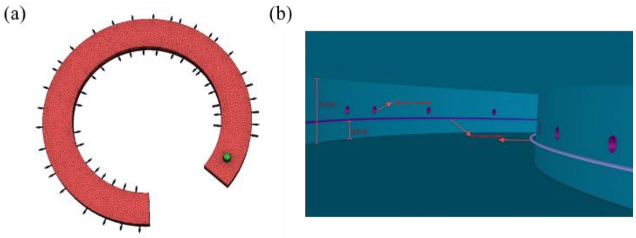

Figure 1. Geometry model of RHF: (a) External structure, (b) Internal structure

2.2 Numerical simulation conditions

2.2.1 Radiative heat transfer

In this paper, after the use of infrared assisted heating, the furnace chamber is mainly through the radiation heat transfer to heat the object, in the case of scattering is not taken into account, in the position $\vec{r}$, the radiative propagation equation (RTE) along the propagation direction $\vec{s}$ is:

$$\frac{dI\left(\vec{r},\vec{s}\right)}{ds} = -aI\left(\vec{r},\vec{s}\right) + aI_b(\vec{r}) \quad (1)$$

Where: $\vec{r}$ is the position vector, $\vec{s}$ is the vector of radiation propagation direction, *a* is the absorption coefficient, *I* is the radiation intensity, $W{\cdot}m^{-2}{\cdot}s{\cdot}r^{-1}$.

The Discrete Ordinates (DO) radiation model is widely employed in numerical simulations of radiative heat transfer to calculate gas-phase radiation across varying optical thicknesses. This method is particularly effective for solving thermal engineering problems involving localized heat sources. Within the model framework, gas absorption coefficients are derived using the Weighted Sum of Gray Gases Model (WSGGM), which enables spectrally resolved estimation of radiation properties for participating media.

2.2.2 Boundary Conditions

The numerical framework incorporated infrared radiation tubes with thermal parameters set to a surface temperature of 1800 K, an emissivity of 0.9, and a radiative flux density of 464,800 W/m². The pellet layer thickness was fixed at 20 mm. Turbulent gas flow was modeled using the k-epsilon turbulence model, selected for its proven efficacy in simulating complex engineering flows. Boundary conditions defined distinct velocity profiles across process zones: thermal air inlets (723 K) were maintained at 21.69 m/s in Reduction Zone V and 30.69 m/s in other sections, while gas injections (300 K) were regulated to 9.59 m/s in Zone V compared to 12.95 m/s elsewhere. The gas composition, rigorously validated against operational data from the referenced steel plant, is systematically presented in Table 1.

Table 1. Volume fraction of gas composition (vol%)

Species	H_2	CO	CH_4	CO_2	N_2
Fraction	13.8	36.4	6.0	17.0	26.6

3. RESULTS AND DISCUSSION

3.1 Temperature field under gas combustion condition

This study conducted numerical simulations to analyze temperature distributions in a rotary hearth furnace under gas combustion heating conditions incorporating infrared radiation modules. Figure 2 illustrates the simulated temperature field profiles. Figure 2 (a) indicates that combustion reactions within the burners produce high-temperature gases with a cross-sectional average temperature of 1510 K. As depicted in Figure 2 (b) and (c), the pellet bed exhibits uniform temperature distribution across the reduction zones, achieving a mean temperature of 1497 K, which meets metallurgical process requirements. Lower temperatures were observed only in the preheating section.

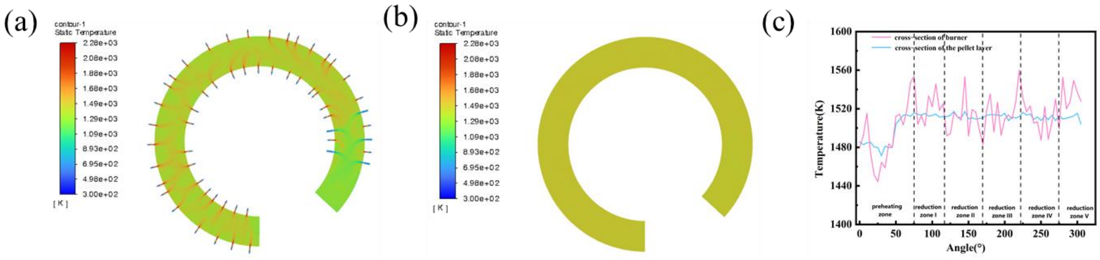

Figure 2. Temperature field: (a) cross−section of burner, (b) and (c) cross−section of the pellet layer.

3.2 Temperature field under infrared heating condition

Numerical simulations of temperature distribution under infrared-only heating conditions were conducted for the rotary hearth furnace model equipped with infrared radiation modules. As shown in Figure 3, the thermal profile within the pellet layer exhibits significantly greater temperature uniformity compared to gas-fired heating configurations. The infrared-assisted system achieved homogeneous thermal distribution with minimal spatial variation, reaching a mean temperature of 1227 K. This improvement stems from the superior heating efficiency of infrared radiation, which facilitates simultaneous surface and core heating of pellets, thereby reducing interfacial temperature gradients.

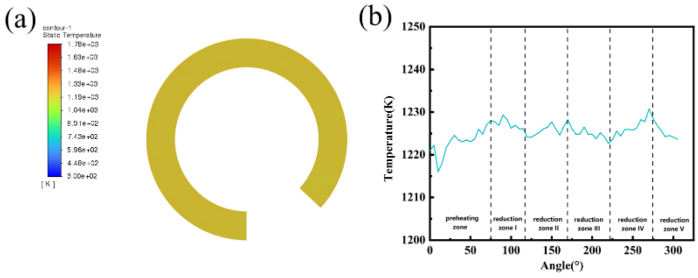

Figure 3. Temperature field ：(a) and (b) cross−section of the pellet layer

3.3 Temperature field under infrared and gas synergistic heating conditions

Numerical simulations of hybrid infrared-gas heating conditions were performed on the rotary hearth furnace, with the resulting thermal and velocity distributions illustrated in Figure 4. Figure 4(a) indicates a cross-sectional mean burner temperature of 1495 K. Figures 4(b) and 4(c) reveal an average pellet bed temperature of 1640 K, representing a 140 K increase over gas-only heating configurations. This improvement significantly enhances heating efficiency and thermal uniformity, attributed to the synergistic coupling of radiative and convective heat transfer mechanisms.

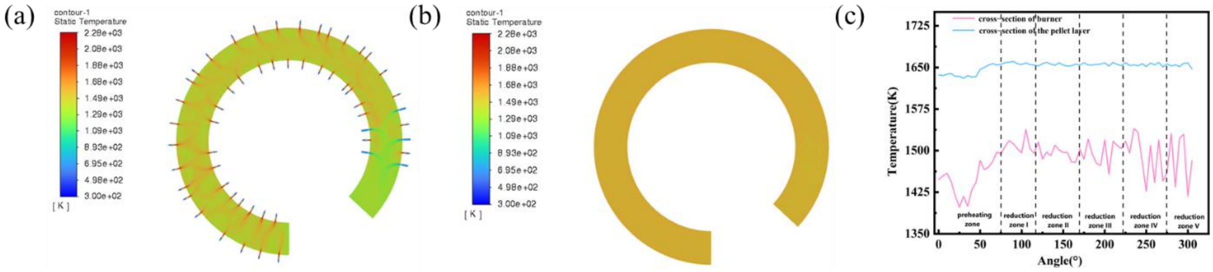

Figure 4. Temperature field: (a) cross−section of burner, (b) and (c) cross−section of the pellet layer

4. CONCLUSIONS

(1) A three-dimensional RHF model was developed in ANSYS Fluent for radiative heat transfer analysis, integrating the k-epsilon turbulence model and the DO radiation framework. Under gas-fired heating conditions, numerical simulations produced a pellet bed mean temperature of 1497 K, aligning with metallurgical process specifications.

(2) Simulations of hybrid infrared-gas heating conditions demonstrated a synergistic thermal enhancement effect, achieving an average pellet layer temperature of 1640 K. This represents a 143 K increase compared to conventional gas heating, significantly improving thermal efficiency and uniformity.

ACKNOWLEDGMENTs

The authors are grateful to the National Key Research and Development Program (2022YFC3901404) for the financial support of this research.

REFERENCES:

[1] J. Kim, M.S. Son, J.K. Park, et al., Fuel Process. Technol., 237 (2022) 107450.
[2] X. He, S.F. Xie, X.F. Li, et al., JOM, 74 (8) (2022) 3039−3048.
[3] P.J. Liu, Z.G. Liu, M.S. Chu, et al., J. Hazard. Mater., 413 (2021) 125403.
[4] D.C. Zhang, R. L. Liu, H. Wang, et al., J. Cent. South Univ., 28 (9) (2021) 2701-2710.
[5] R. Bayoumi, N.M. Abdelmonem, M.A. Soliman, et al., Proceedings of 11th International Conference on Chemical and Environmental Engineering, Cairo, Egypt, 2022.
[6] X.L. Lin, Z.W. Peng, J.X. Yan, et al., J. Clean. Prod., 149 (2017) 1079-1100.
[7] X.F. She, J.S. Wang, G. Wang, et al., J. Iron Steel Res. Int., 21 (5) (2014) 488-495.
[8] H. Tsutsumi, S. Yoshida, M. Tetsumoto, R&D Kobe Steel Eng. Rep., 60 (1) (2010) 36-42.
[9] K. Myroniuk, V. Shepitchak, Y. Furdas, et al., Constr. Optim. Energy Potential, 13 (1) (2024) 129-142.
[10] D. Mauduit, M. Le Fournier, K. Grondin, et al., Proceedings of International Conference on Technology of Plasticity, Cambridge, UK, 2017, p.1904-1909.